

Article

Petrogenesis and Geological Significance of the Quartz Monzonites in the Jinling Area, Western Shandong Province

Zhao-Lu Zhang ^{1,2}, Chao Zhang ^{1,2,*}, Ye Li ¹, Lu-Yuan Wang ¹, Ji-Lei Gao ^{2,3}, Ming Ma ^{2,3} and Ya-Dong Li ^{2,3}

¹ The School of Resources and Environmental Engineering, Shandong University of Technology, Zibo 255049, China; zhzh1@sdut.edu.cn (Z.-L.Z.); 18753377965@163.com (Y.L.); wangluyuan9@163.com (L.-Y.W.)

² Shandong Engineering Laboratory for High-Grade Iron Ore Exploration and Exploitation, Jinan 250100, China; gjln@163.com (J.-L.G.); sddkmaming@163.com (M.M.); li987654202205@163.com (Y.-D.L.)

³ No. 1 Institute of Geology and Mineral Resources of Shandong Province, Jinan 250100, China

* Correspondence: czhang@sdut.edu.cn

Abstract: Jinling complex pluton is a key part of the Mesozoic magmatic belt in the eastern North China Craton. However, its petrogenesis is still being debated. The Jinling complex, mainly composed of biotite diorites, hornblende diorite, augite diorites, (quartz) monzonites, and quartz diorites, is outcropped in Huashan and Heitieshan. This paper studies the zircon geochronology, zircon Hf isotope, and Sr-Nd-Pb isotope of quartz monzonites. The samples have high contents of Cr, Ni, V, Al₂O₃, Ba, Sr, and are enriched in LREEs, LILEs (K, Ba, Sr), depleted in HREEs, and HFSEs (Nb, Ta, Ti). The samples with captured zircons of ~2.5 Ga yield a weighted mean age of ~127 Ma, and the zircons have negative values of $\epsilon_{\text{Hf}}(t)$ from -3.2 to -9.4 while the ratios of ²⁰⁸Pb/²⁰⁴Pb, ²⁰⁷Pb/²⁰⁴Pb, ²⁰⁶Pb/²⁰⁴Pb 37.75~38.15, 15.41~15.43, 17.59~17.98, respectively. The ratios of Th/U are from 3.77 to 3.82, while the values of μ and ω are 9.18 and from 35.72 to 36.15. Meanwhile, the ratios of ⁸⁷Sr/⁸⁶Sr are higher than the ones of the mantle. Geochemical and isotopic features indicate that the quartz monzonites derived from the subcontinental lithospheric mantle that probably assimilated ancient NCC upper crust materials (~15–20%) during the magma ascent in a lithospheric extension setting.

Keywords: zircon U-Pb geochronology; zircon Hf isotope; Sr-Nd-Pb isotopes; Western Shandong province; North China Craton



Citation: Zhang, Z.-L.; Zhang, C.; Li, Y.; Wang, L.-Y.; Gao, J.-L.; Ma, M.; Li, Y.-D. Petrogenesis and Geological Significance of the Quartz Monzonites in the Jinling Area, Western Shandong Province. *Minerals* **2022**, *12*, 771. <https://doi.org/10.3390/min12060771>

Academic Editors: Sergei Khromykh and Andrei Tsygankov

Received: 7 May 2022
Accepted: 15 June 2022
Published: 17 June 2022

Publisher's Note: MDPI stays neutral with regard to jurisdictional claims in published maps and institutional affiliations.



Copyright: © 2022 by the authors. Licensee MDPI, Basel, Switzerland. This article is an open access article distributed under the terms and conditions of the Creative Commons Attribution (CC BY) license (<https://creativecommons.org/licenses/by/4.0/>).

1. Introduction

The lithospheric thinning and destruction of Craton are remarkable in the North China Craton during the Mesozoic period and are significantly accountable for extensive tectonic-magmatic-mineralization processes [1]. Therefore, it is a hot topic for the discussion of the petrogenesis and tectonic setting of Mesozoic magmatic rocks in eastern China Craton [2–6]. The Cretaceous Jinling complex, with a square of 80 km², is situated to the east of Zibo City, Shandong province. The Jinling complex intruded Middle Ordovician formation and Lower Carboniferous formation and is described as an important factor of skarn Fe deposit in the Jinling area, Zibo City, as well as a key part of the Mesozoic magmatic belt in the eastern part of the North China Craton. However, in the academic domain, there are still different opinions on the magmatic source and the petrogenesis of the Jinling complex pluton in western Shandong province, including (1) partial melts of delaminated continental lower crust interacting with mantle peridotite, (2) partial melts of enriched lithospheric mantle previously metasomatized by subducted or delaminated continental crust, (3) magma mixing between siliceous crustal melts and basaltic magmas from metasomatized mantle assimilation of the previous emplacement, and (4) mantle peridotite by crust-derived monzodioritic magmas at crustal depth. Yang et al. (2006) [7] reported the zircon U-Pb dating, geochemistry, and Sr-Nd isotopic data of the biotite diorites. The results show that

the rocks could be formed in the interaction between the detachment of the Yangtze Craton subduction plate and the delamination of the North China Craton, and the rocks are the mixed melting products of the delamination lithosphere and the asthenosphere based on the Sr-Nd isotopic components similar to the primitive mantle and high REE components. Zhong et al. (2012) [8] analyzed the high $\epsilon_{\text{Hf}}(t)$ values and young Hf isotopic model age of depleted mantle and deemed that the magma of Jinling pluton originated from ancient enriched lithospheric mantle influenced by upwelling mantle material that was caused by Tan–Lu Fault activity. Considering the negative Hf isotopic component, low initial $^{87}\text{Sr}/^{86}\text{Sr}$ ratios, and high ϵ_{Nd} values, Jin et al. (2015) [9] held that the magma of the Jinling pluton was the product of the action between delaminated continental lower crust and mantle peridotite and the magma was multistage emplaced and mixed by continental crust during its evolution. Lan et al. (2019) [10] found the Jinling pluton had high $\text{Mg}^\#$ values, trace elements similar to island arc magma, and the Sr-Nd-Pb isotopic components between the lithospheric mantle and ancient crust, indicating the magma derived from the metasomatic hydrated the continental lithospheric mantle with crustal contamination. Combined with the previous studies, Lan et al. (2019) [10] further deemed that the Jinling pluton was emplaced under an extensional tectonic setting, which was formed by asthenosphere upwelling caused by the ancient Pacific detention plate. However, the Jinling complex has a close relationship with the skarn-type iron ore deposit, and its magmatic attribute is an important way to understand the metallogenic mechanism of the skarn-type iron ore deposit. Thereby, it is necessary to discuss the petrogenesis of Mesozoic pluton in the Jinling area, western Shandong province. In view of this, the paper studied the zircon U-Pb dating, geochemistry, and Sr-Nd-Pb-Hf isotopes in order to discuss the magmatic source, petrogenesis, and emplacing age and the tectonic setting.

2. Geological Background and Sample Description

Shandong province is located in the southeast of North China Craton and divided into two parts including west Shandong Province and the Jiaodong area. West Shandong province, located to the west of the Tan–Lu fault belt (Figure 1a,b), is bounded by the Lankao–Liaocheng fault to the west, the Qihe–Guangrao fault to the north, and the Sulu–Dbie ultra-high-pressure metamorphic belt to the southeast [11] and has experienced multistage tectonic thermal events, such as Ivliang, Caledonian, Hercynian movement, etc. The stratum in this area is composed of a Precambrian basement and Paleozoic and Mesozoic strata, while the magmatic events are divided into Yishui, Lushan–Yishan, Taishan–Aolaishan–Menshan, and Mashan–Lingshan–Sihaishan intrusive magmatic belts and Weifang–Tancheng volcanic magmatic belts according to the temporal and spatial distribution characteristics. Furthermore, Mesozoic magmatic events consist of Late Triassic alkaline rock, Middle–Late Jurassic granitic rocks, Early Cretaceous diorites-granodiorites, and Late Cretaceous alkaline basalt. Western Shandong Province has a similar tectonic evolution to the North China Craton. However, the basic geological framework of NCC was formed in the Paleoproterozoic. In the Paleozoic, the tectonic evolution of western Shandong province was influenced by the collision between the NCC and Yangtze Craton. Therefore, a set of marine strata were deposited during the Early Paleozoic period, and a set of continental strata were deposited during Late Paleozoic NCC. The Mesozoic and Cenozoic are the key periods for lithospheric thinning and tectonic transition in western Shandong Province. Under the extensional setting of NCC, western Shandong Province was characterized by massive magmatic activities and graben basins in the Early Cretaceous.

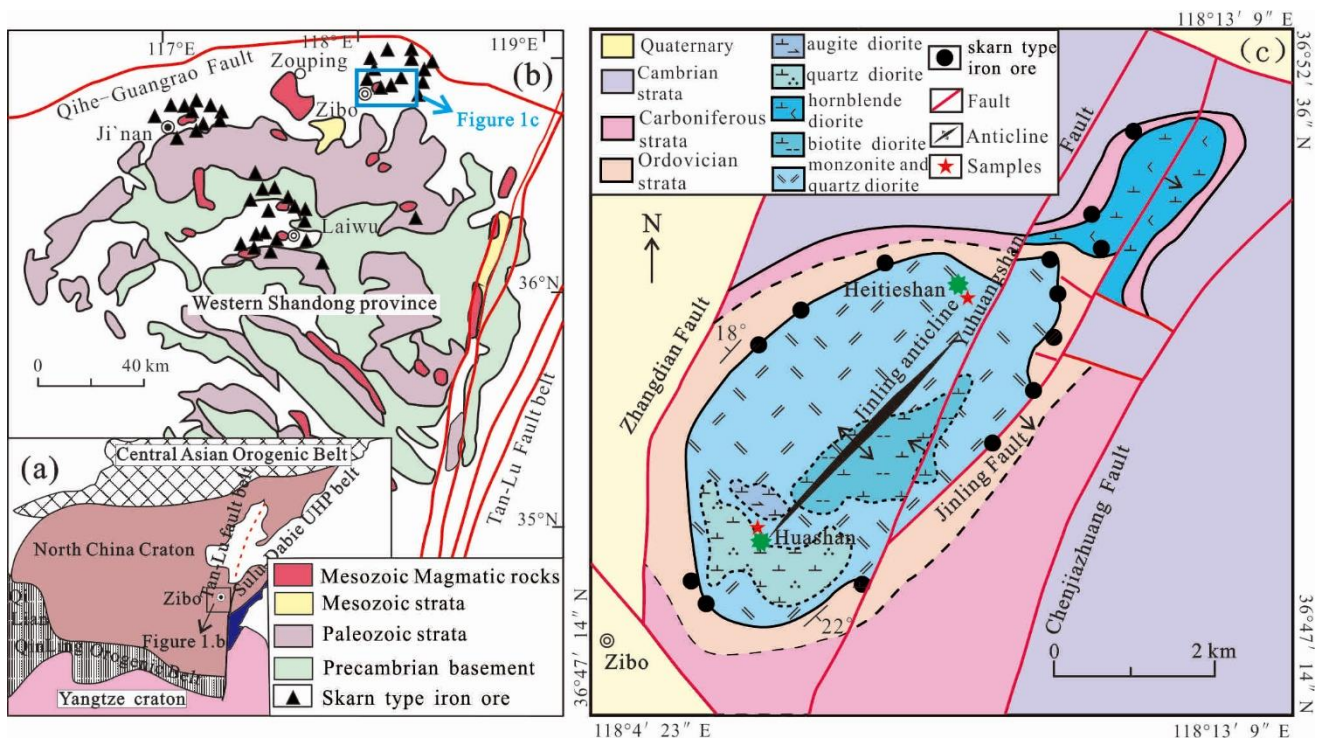


Figure 1. (a) The tectonic location of western Shandong area; (b) simplified geological map of western Shandong area; (c) simplified geological map of Jinling pluton in western Shandong province (modified after reference [11]). Cambrian strata are composed of shales and limestones, Carboniferous strata are composed of shales and slates, and Ordovician strata are composed of limestones. Mesozoic strata are composed of Triassic and Jurassic sandstones and shales, while Paleozoic strata are composed of Cambrian strata, Ordovician strata, and Carboniferous strata.

Jinling area is located in the north of western Shandong province. Middle Ordovician Majiagou formation and Lower Carboniferous Benxi formation outcropped in this area and intruded the Jinling complex. The Jinling complex, mainly composed of biotite diorites, hornblende diorite, augite diorites, monzonites and quartz diorites, outcropped in Huashan and Heitieshan (Figure 1c). The complex main body is monzonite, biotite diorite, quartz diorite and augite diorite. Amphibole diorite is mainly developed in the northeast direction of monzonite. According to the previous studies, monzonite and hornblende diorite are connected in the deep [9]. The faults, including the Zhangdian fault, Yuhuangshan fault, Jinling fault, and Chenjiashuang fault, are mainly in the direction of NNE, and the anticline structure is also in the direction of NNE.

In this study, the monzonites are collected from Jinling pluton. The sample HS4 was from Huashan, while HTS3 and HTS5 were from Heitieshan. The sample HZ7 was from −300 m of mine tunnel near Heitieshan underground. The fine-middle quartz monzonites are mainly composed of quartz (17%), alkali feldspar (10%), plagioclase (67%), and biotite (6%) (Figure 2). However, the amphibole is also discovered in the Sample HTS3 (Figure 2d).



Figure 2. Petrological features of Quartz monzonites in the Jinling area, western Shandong province. (a,b)—HS4, quartz monzonites; (c,d)—HTS3, quartz monzonites. Q—Quartz; Bi—Biotite, Amp—Amphibole, Pl—Plagioclase.

3. Analytical Methods

3.1. Zircon U-Pb Dating and Situ Hf Isotope Analysis

Zircon grains were selected from two samples (HTS3 and HS4) using conventional heavy liquid and magnetic techniques at the Langfang Geological Survey, Hebei province, China. Under the binocular microscope, parts of zircon grains were mounted on the resin disc and then were polished to expose the zircon grain surface. Cathodoluminescence (CL) images were obtained in order to obtain the internal structures prior to analysis. LA-ICP-MS zircon U-Pb and Hf isotope analyses were performed at the Beijing YanduZhongshi Testing Technology Corporation.

Zircon dating results were obtained on an M90 LA-MC-ICPMS made by German Jena Corporation with a 193 nm laser. In the analysis process, helium and argon were used as carrier gas and compensation gas, respectively, to adjust the sensitivity. The spot diameter is 35 μm , and the denudation depth ranges from 20 to 40 μm . Furthermore, 91,500 and plesovice act as the standards for optimizing the analysis [12,13]. The method of Anderson is used to correct common Pb, and Errors on individual analysis by LA-ICP-MS were quoted at the 1σ level, while errors on pooled ages were quoted at the 95% (2σ) confidence level. Concorde diagram and weighted average age were finished with IsoplotR [14].

Zircon Hf isotopic analyses were finished using a Neptune-plus MC-ICPMS, equipped with a 193 nm laser. The Hf isotopic analysis was carried out for 31 s at a beam density of 16 J/cm² and at 8Hz with a spot size of 35 μm . The detailed test process has been described by Wu et al. (2006) [15]. The calculation method and formula could be referenced from Wu et al. (2007) [16]. Parameters are listed below: $(^{176}\text{Lu}/^{177}\text{Hf})_{\text{CHUR}} = 0.0332$, $(^{176}\text{Hf}/^{177}\text{Hf})_{\text{CHUR}} = 0.282772$, $(^{176}\text{Lu}/^{177}\text{Hf})_{\text{DM}} = 0.0384$, $(^{176}\text{Hf}/^{177}\text{Hf})_{\text{DM}} = 0.28325$, Lu decay constant (λ) = $1.865 \times 10^{-11} \text{a}^{-1}$, and $^{176}\text{Lu}/^{177}\text{Hf} = -0.34$.

3.2. Whole-Rock Elemental Analysis

Samples were selected for whole-rock geochemical data (major and trace elements) at the Guizhou Tongwei Analytical Technology Corporation.

Fresh samples were crushed and powdered to ~200 mesh, and a sample weighted over 1g was used to obtain the geochemical data with the X-ray fluorescence (ARL Perform'X 4200) made by Thermo Fisher Corporation. Rare earth elements and trace elements data were analyzed with ICP-MS (Perkin Elmer Elan 6000) and ICP-AES, respectively. Sample solutions were diluted 4000 times and added to 6ppb Rh, In, Re, and Bi internal spikes. USGS W-2a was used as a reference standard and cross-checked with BHVO-2 or other reference materials. Instrument drift mass bias were corrected with internal spikes and external monitors. The results and relative standard deviations are in ppb and 1 sigma.

3.3. Whole-Rock Sr-Nd-Pb Isotope Analysis

The whole-rock Sr-Nd-Pb isotopic analysis was conducted at the Guizhou Tongwei Analytical Technology Corporation. Sr isotopic analysis was performed on VG Sector 54 using a TRITON thermal ionization mass spectrometer instrument. The fractionation method was corrected with a value of $^{86}\text{Sr}/^{88}\text{Sr}$ (0.1194). NBS⁹⁸⁷ was used as the instrument status monitor, while NBS-987 was the average value of the corrected sample. Nd and Pb isotopes were analyzed on Nu Plasma HR MC-ICP-MS. The detailed procedure followed with references [17–19].

The operation parameters are listed below: $^{146}\text{Nd}/^{144}\text{Nd} = 0.7219$, $\text{JNdI-1}^{143}\text{Nd}/^{144}\text{Nd} = 0.512113 \pm 9$, $^{208}\text{Pb}/^{204}\text{Pb} = 36.7071 \pm 79$, $^{207}\text{Pb}/^{204}\text{Pb} = 15.4944 \pm 22$, $^{206}\text{Pb}/^{204}\text{Pb} = 16.9370 \pm 31$, $^{208}\text{Pb}/^{206}\text{Pb} = 2.16729 \pm 16$, and $^{207}\text{Pb}/^{206}\text{Pb} = 0.91483 \pm 6$.

4. Analytical Results

The LA-ICPMS zircons U-Pb data (HS4 and HTS3) are listed in Table 1, while zircon Hf isotope data are listed in Table 2, respectively.

Table 1. LA-ICP-MS zircon U-Pb data of quartz monzonites from the Jinling complex pluton in western Shandong province.

No.	Th ($\times 10^{-6}$)	U ($\times 10^{-6}$)	Th/U	U-Pbisotopicratios						Age (Ma)					
				$^{207}\text{Pb}/^{206}\text{Pb}$	1 σ	$^{207}\text{Pb}/^{235}\text{U}$	1 σ	$^{206}\text{Pb}/^{238}\text{U}$	1 σ	$^{208}\text{Pb}/^{232}\text{Th}$	1 σ	$^{207}\text{Pb}/^{206}\text{U}$	1 σ	$^{206}\text{Pb}/^{238}\text{U}$	1 σ
HS4															
1	2418	925	2.61	0.0523	0.0015	0.1422	0.0044	0.0197	0.0004	0.0064	0.0001	532	95	126	3
2	190	133	1.43	0.0466	0.0038	0.1273	0.0107	0.0197	0.0005	0.0061	0.0003	185	84	126	3
3	156	121	1.29	0.0509	0.0025	0.1396	0.0072	0.0200	0.0004	0.0067	0.0003	267	85	127	3
4	97	85	1.14	0.0489	0.0055	0.1384	0.0162	0.0203	0.0005	0.0065	0.0005	180	105	129	3
5	363	199	1.83	0.0535	0.0020	0.1294	0.0048	0.0177	0.0002	0.0056	0.0001	196	66	113	2
6	176	149	1.18	0.0516	0.0042	0.1504	0.0132	0.0207	0.0008	0.0084	0.0007	122	78	132	5
7	265	174	1.52	0.0502	0.0031	0.1396	0.0088	0.0202	0.0005	0.0068	0.0003	167	70	129	3
8	2262	725	3.12	0.1388	0.0043	0.4056	0.0195	0.0208	0.0005	0.0063	0.0002	42	79	132	3
9	2758	1027	2.68	0.0501	0.0016	0.1350	0.0041	0.0195	0.0004	0.0061	0.0001	317	106	125	2
10	113	83	1.35	0.0519	0.0045	0.1367	0.0108	0.0201	0.0004	0.0063	0.0003	187	98	128	3
11	2845	999	2.85	0.0494	0.0011	0.1357	0.0037	0.0198	0.0003	0.0059	0.0001	192	100	126	2
12	314	152	2.07	0.0463	0.0028	0.1289	0.0094	0.0199	0.0005	0.0062	0.0003	118	144	127	3
13	169	110	1.53	0.0514	0.0037	0.1408	0.0109	0.0201	0.0005	0.0069	0.0003	318	113	128	3
14	2383	980	2.43	0.0508	0.0018	0.1386	0.0046	0.0199	0.0003	0.0062	0.0002	142	98	127	2
15	1500	981	1.53	0.0492	0.0011	0.1360	0.0033	0.0200	0.0002	0.0066	0.0001	244	67	128	2
16	226	140	1.61	0.0496	0.0033	0.1363	0.0090	0.0202	0.0005	0.0066	0.0003	134	83	129	3
17	398	208	1.91	0.0508	0.0022	0.1384	0.0057	0.0201	0.0003	0.0060	0.0002	137	77	128	2
18	695	414	1.68	0.0496	0.0016	0.1483	0.0048	0.0217	0.0003	0.0070	0.0001	293	97	138	2
19	1136	534	2.13	0.0502	0.0017	0.1361	0.0046	0.0196	0.0003	0.0061	0.0002	202	81	125	2
20	459	260	1.77	0.0474	0.0021	0.1288	0.0060	0.0198	0.0004	0.0064	0.0002	212	86	126	2
21	214	140	1.53	0.0486	0.0030	0.1330	0.0082	0.0201	0.0003	0.0069	0.0005	281	95	128	2
22	488	229	2.13	0.0474	0.0022	0.1282	0.0061	0.0198	0.0003	0.0063	0.0001	179	104	126	2
23	47	40	1.17	0.0530	0.0052	0.1415	0.0133	0.0202	0.0005	0.0064	0.0004	162	83	129	3
24	662	304	2.17	0.0495	0.0017	0.1345	0.0048	0.0197	0.0003	0.0064	0.0002	156	108	126	2

Table 1. Cont.

No.	Th ($\times 10^{-6}$)	U ($\times 10^{-6}$)	Th/U	U-Pb isotopic ratios						Age (Ma)					
				$^{207}\text{Pb}/^{206}\text{Pb}$	1 σ	$^{207}\text{Pb}/^{235}\text{U}$	1 σ	$^{206}\text{Pb}/^{238}\text{U}$	1 σ	$^{208}\text{Pb}/^{232}\text{Th}$	1 σ	$^{207}\text{Pb}/^{206}\text{U}$	1 σ	$^{206}\text{Pb}/^{238}\text{U}$	1 σ
HTS3															
1	1063	447	2.38	0.0485	0.0018	0.1340	0.0048	0.0201	0.0003	0.0074	0.0003	121	86	128	2
2	3136	962	3.26	0.0480	0.0009	0.1302	0.0028	0.0196	0.0002	0.0071	0.0001	99	45	125	2
3	2425	840	2.89	0.0479	0.0014	0.1317	0.0041	0.0198	0.0003	0.0070	0.0002	93	71	127	2
4	986	481	2.05	0.0486	0.0012	0.1318	0.0032	0.0197	0.0002	0.0071	0.0002	128	59	126	1
5	3913	1014	3.86	0.0468	0.0009	0.1280	0.0027	0.0198	0.0003	0.0068	0.0002	41	48	126	2
6	944	449	2.10	0.0485	0.0013	0.1332	0.0036	0.0199	0.0003	0.0068	0.0002	126	65	127	2
7	814	468	1.74	0.0478	0.0014	0.1293	0.0037	0.0198	0.0002	0.0066	0.0001	87	70	126	1
8	1048	441	2.38	0.0494	0.0012	0.1398	0.0038	0.0206	0.0003	0.0068	0.0002	165	59	131	2
9	2924	866	3.38	0.0486	0.0010	0.1324	0.0031	0.0197	0.0002	0.0064	0.0001	130	50	126	2
10	760	487	1.56	0.0479	0.0015	0.1302	0.0040	0.0197	0.0002	0.0062	0.0001	96	72	126	1
11	1413	587	2.41	0.0476	0.0020	0.1289	0.0053	0.0197	0.0003	0.0066	0.0001	80	98	126	2
12	1054	437	2.41	0.0483	0.0017	0.1314	0.0044	0.0198	0.0002	0.0063	0.0001	116	84	126	1
13	823	419	1.97	0.0484	0.0012	0.1318	0.0035	0.0199	0.0002	0.0062	0.0002	117	60	127	1
14	680	488	1.39	0.0489	0.0013	0.1325	0.0039	0.0196	0.0002	0.0065	0.0001	145	63	125	1
15	1515	526	2.88	0.0484	0.0010	0.1317	0.0030	0.0198	0.0002	0.0062	0.0002	117	50	126	1
16	767	474	1.62	0.0477	0.0015	0.1312	0.0047	0.0199	0.0003	0.0062	0.0002	85	74	127	2
17	203	354	0.57	0.1664	0.0020	10.2288	0.1927	0.4446	0.0067	0.1235	0.0018	2521	20	2371	30
18	526	429	1.23	0.0494	0.0024	0.1350	0.0064	0.0200	0.0004	0.0066	0.0002	169	114	128	2
19	1245	490	2.54	0.0489	0.0014	0.1369	0.0041	0.0204	0.0003	0.0068	0.0002	144	67	130	2
20	2107	619	3.40	0.0485	0.0012	0.1318	0.0036	0.0197	0.0003	0.0060	0.0002	123	60	126	2
21	1144	436	2.62	0.0487	0.0015	0.1326	0.0044	0.0198	0.0003	0.0062	0.0002	136	70	126	2
22	1103	446	2.48	0.0480	0.0014	0.1359	0.0044	0.0206	0.0003	0.0066	0.0002	101	67	131	2
23	944	413	2.29	0.0484	0.0018	0.1325	0.0056	0.0197	0.0003	0.0064	0.0002	117	90	126	2
24	98	121	0.81	0.1671	0.0015	11.0817	0.1780	0.4796	0.0057	0.1345	0.0042	2528	15	2525	25

Table 2. Zircon Hf isotopic compositions of quartz monzonites from the Jinling area, western Shandong province.

No.	Age (Ma)	$^{176}\text{Yb}/^{177}\text{Hf}$	$^{176}\text{Lu}/^{177}\text{Hf}$	$^{176}\text{Hf}/^{177}\text{Hf}$	2 σ	$^{176}\text{Hf}/^{177}\text{Hf}$	$\epsilon_{\text{Hf}}(0)$	$\epsilon_{\text{Hf}}(t)$	T_{DM} (Ma)	T_{DM}^{C} (Ma)	$f_{\text{Lu/Hf}}$
HS4-3	126	0.055800	0.001661	0.282555	0.000020	0.282551	-7.7	-5.1	1006	2078	-0.95
HS4-4	127	0.038858	0.001185	0.282473	0.000018	0.282470	-10.6	-7.9	1108	2333	-0.96
HS4-5	129	0.025070	0.000724	0.282521	0.000017	0.282519	-8.9	-6.1	1027	2174	-0.98
HS4-8	129	0.047770	0.001432	0.282533	0.000019	0.282530	-8.4	-5.7	1030	2141	-0.96
HS4-10	125	0.071451	0.002012	0.282596	0.000016	0.282591	-6.2	-3.6	955	1950	-0.94
HS4-11	128	0.028365	0.000868	0.282582	0.000015	0.282580	-6.7	-4.0	946	1984	-0.97
HS4-13	127	0.018211	0.000537	0.282513	0.000017	0.282512	-9.2	-6.4	1034	2201	-0.98
HS4-14	128	0.045227	0.001253	0.282605	0.000015	0.282602	-5.9	-3.2	923	1913	-0.96
HS4-17	129	0.048596	0.001390	0.282595	0.000019	0.282592	-6.3	-3.6	941	1944	-0.96
HS4-18	128	0.051944	0.001431	0.282567	0.000017	0.282564	-7.2	-4.6	982	2035	-0.96
HTS3-1	128	0.138895	0.003818	0.282546	0.000021	0.282537	-8.0	-5.5	1080	2118	-0.88
HTS3-2	125	0.160725	0.004239	0.282490	0.000022	0.282480	-10.0	-7.6	1179	2302	-0.87
HTS3-3	127	0.174687	0.004831	0.282534	0.000021	0.282522	-8.4	-6.0	1132	2166	-0.85
HTS3-6	127	0.170495	0.004752	0.282440	0.000023	0.282428	-11.8	-9.4	1276	2464	-0.86
HTS3-7	126	0.102291	0.002935	0.282478	0.000019	0.282471	-10.4	-7.9	1155	2331	-0.91
HTS3-9	126	0.099879	0.002814	0.282448	0.000022	0.282442	-11.4	-8.9	1194	2423	-0.92
HTS3-10	126	0.118492	0.003490	0.282458	0.000023	0.282450	-11.1	-8.6	1202	2397	-0.89
HTS3-11	126	0.157885	0.004131	0.282541	0.000023	0.282531	-8.2	-5.8	1098	2140	-0.88
HTS3-14	125	0.124968	0.003785	0.282463	0.000020	0.282454	-10.9	-8.5	1206	2386	-0.89
HTS3-21	126	0.146769	0.003949	0.282513	0.000022	0.282504	-9.1	-6.7	1134	2226	-0.88

4.1. LA-ICPMS Zircon U-Pb Ages

Zircons' age and CL images of Sample HS4 and HTS3 are presented in Figure 3.

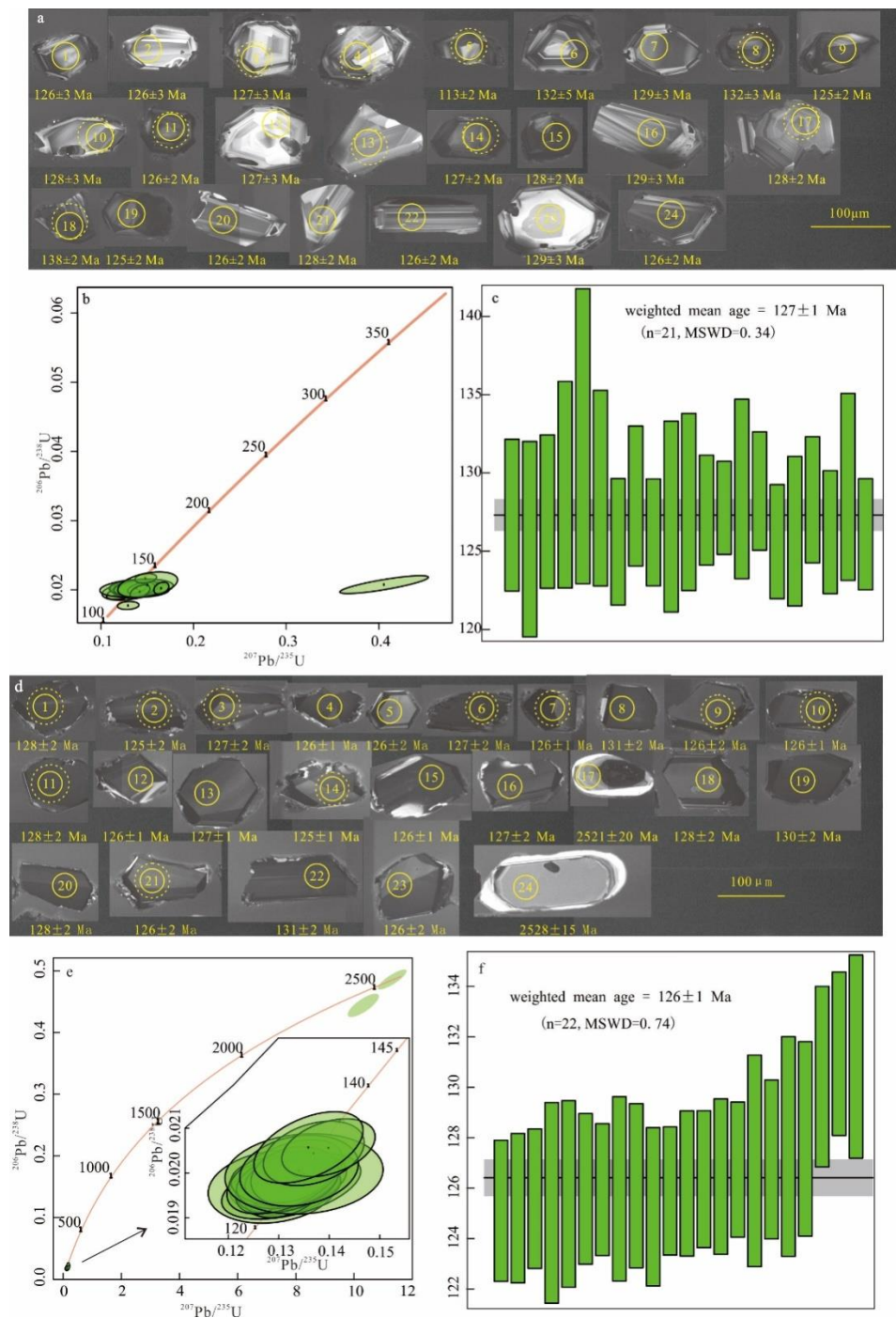


Figure 3. CL pictures (a,d), U-Pb Concorde diagrams (b,e), and zircon U-Pb weighted mean age (c,f) of zircons of quartz monzonites ((a–c)–HS4, (d–f)–HTS3) from the Jinling area, western Shandong province.

4.1.1. Quartz Monzonite (Sample HS4)

Twenty-four zircons from HS4 have a length ranging from 50 μm to 100 μm and display fine-scale oscillatory growth zoning in CL images, indicating the features of the magmatic zircons (Figure 3a). The contents of Th and U range from 46.65×10^{-6} to 2844.59×10^{-6} and from 39.95×10^{-6} to 1027.13×10^{-6} , respectively, while the ratios of Th/U are from 1.14 to 3.12 (Table 1). Three data are not calculated because of their far distance from the Concorde line. Surface ages of the remaining 21 zircons range from $125 \pm 2 \text{ Ma}$ – $132 \pm 5 \text{ Ma}$ and yield a weight mean age of $127 \pm 1 \text{ Ma}$ ($n = 21$, MSWD = 0.36;

Figure 3c). However, this age is from magmatic zircons with oscillatory growth zoning, thus could be interpreted as the crystallization age of the quartz monzonite.

4.1.2. Quartz Monzonite (Sample (HTS3))

Zircons in sample HTS3 could be divided into two groups based on zircon morphology. One group, with a narrow metamorphic edge, is characterized by a rounded shape with a length from 100 μm to 150 μm . These zircons have an age of 2521–2528 Ma, suggesting that they are xenocrystic zircons. The other group is mainly subhedral, and the zircons with lengths ranging from 50 μm to 120 μm display streak or oscillatory growth zoning in CL images (Figure 3d). All the zircon ages are plotted on or near the Concorde line, while two zircon grains have Archean ages. The Th contents of Cretaceous twenty-two zircons range from 526×10^{-6} to 3913×10^{-6} , while the U contents range from 121×10^{-6} to 1014×10^{-6} . However, the zircons have $^{206}\text{Pb}/^{238}\text{U}$ ages ranging from 125 ± 1 Ma to 131 ± 2 Ma and yield a weighted mean age of 126 ± 1 Ma (MSWD = 0.74, $n = 22$) (Figure 3e,f). This age is consistent with that of sample HS4 and could be considered as the emplacing age of Jinling pluton.

4.2. Zircon Hf Isotopic Compositions

A total of 20 zircon ages from two samples (HS4, HTS3) are used for Hf isotope analysis. The values of $^{176}\text{Lu}/^{177}\text{Hf}$ in ten spots from sample HS4 are from 0.000537 to 0.002012, while the initial values of $^{176}\text{Hf}/^{177}\text{Hf}$ range from 0.282471 to 0.282562. Their $\varepsilon_{\text{Hf}}(t)$ and T_{DM1} values vary from -3.2 to -7.8 and from 1915 Ma to 2329 Ma, respectively. Ten zircons from sample HTS3 are dated for Hf isotopic compositions, with $^{176}\text{Lu}/^{177}\text{Hf}$ ratios of 0.002814–0.004831, initial $^{176}\text{Hf}/^{177}\text{Hf}$ ratios of 0.282428–0.282537, $\varepsilon_{\text{Hf}}(t)$ values of -5.5 to -9.4 , and T_{DM1} values of 1080–1276 Ma, respectively.

4.3. Major and Trace Elements

Four samples were analyzed to obtain the geochemical features of the Early Cretaceous quartz monzonites in the study area. The geochemical data have been listed in Table 3.

Table 3. The chemical compositions of major elements (%), trace elements ($\times 10^{-6}$), and REE elements of quartz monzonites from the Jinling area, western Shandong province.

Sample	HZ7	HS4	HTS3	HTS5	Sample	HZ7	HS4	HTS3	HTS5
SiO ₂	63.72	66.06	64.28	65.04	Er	1.07	1.08	1.12	0.98
TiO ₂	0.51	0.58	0.56	0.56	Tm	0.16	0.15	0.17	0.15
Al ₂ O ₃	14.04	16.86	14.99	15.55	Yb	0.95	0.89	1.03	0.93
Fe ₂ O ₃	4.24	2.69	4.12	2.21	Lu	0.15	0.12	0.16	0.15
MnO	0.05	0.04	0.06	0.05	Y	11.40	11.80	12.00	10.50
MgO	3.74	0.77	2.97	2.65	Ba	822.00	1430.00	1080.00	1330.00
CaO	3.56	2.33	3.72	3.84	Rb	49.40	87.90	63.10	74.20
Na ₂ O	5.38	4.69	4.96	4.74	Sr	529.00	433.00	601.00	625.00
K ₂ O	2.78	4.86	3.76	4.74	Zr	149.00	92.00	183.00	178.00
P ₂ O ₅	0.21	0.11	0.22	0.21	Nb	6.24	13.60	7.20	6.14
LOI	0.84	1.14	0.60	0.77	Ni	72.90	15.10	58.80	50.60
Total	99.07	100.13	100.24	100.36	Co	13.60	6.69	11.90	8.92
La	22.30	43.10	23.30	21.90	Zn	27.60	27.20	41.90	34.90
Ce	47.10	72.50	45.40	40.80	Cr	173.00	145.00	122.00	118.00
Pr	5.80	7.94	5.39	4.88	Cs	0.32	0.98	0.50	0.49
Nd	22.80	27.20	21.10	18.60	Ta	0.37	1.24	0.44	0.43
Sm	4.23	4.40	4.02	3.40	Hf	3.69	3.23	4.46	4.29
Eu	1.14	1.46	1.12	1.07	Th	4.86	7.89	5.85	5.33
Gd	3.66	3.95	3.54	3.07	Li	6.74	31.90	12.60	12.40
Tb	0.45	0.48	0.45	0.38	v	85.00	58.40	86.60	61.30
Dy	2.17	2.29	2.21	1.91	Mg [#]	64.00	36.00	58.00	70.00
Ho	0.40	0.41	0.42	0.36	σ	3.21	3.96	3.57	4.08

Note: $\text{Mg}^{\#} = 100[w(\text{MgO})/40.31]/[w(\text{MgO})/40.31 + w(\text{TFeO})/71.85]$, the ' σ ' represents for the Rittman index.

All the samples are plotted in the quartz monzonites field in the TAS diagram (Figure 4a) and in the high-K calc-alkaline series and shoshonite series field in the $\text{SiO}_2\text{-K}_2\text{O}$ diagram (Figure 4b). The quartz monzonites have the content of SiO_2 , Fe_2O_3^T , MgO , Al_2O_3 , CaO , Na_2O , and K_2O ranging from 63.72% to 66.06%, from 2.21% to 4.24%, from 0.74% to 3.74%, from 14.04% to 16.86%, from 2.33% to 3.84%, from 4.69% to 5.38%, and from 2.78% to 4.86%. Furthermore, the Rittmann indexes of samples range from 3.21 to 4.08.

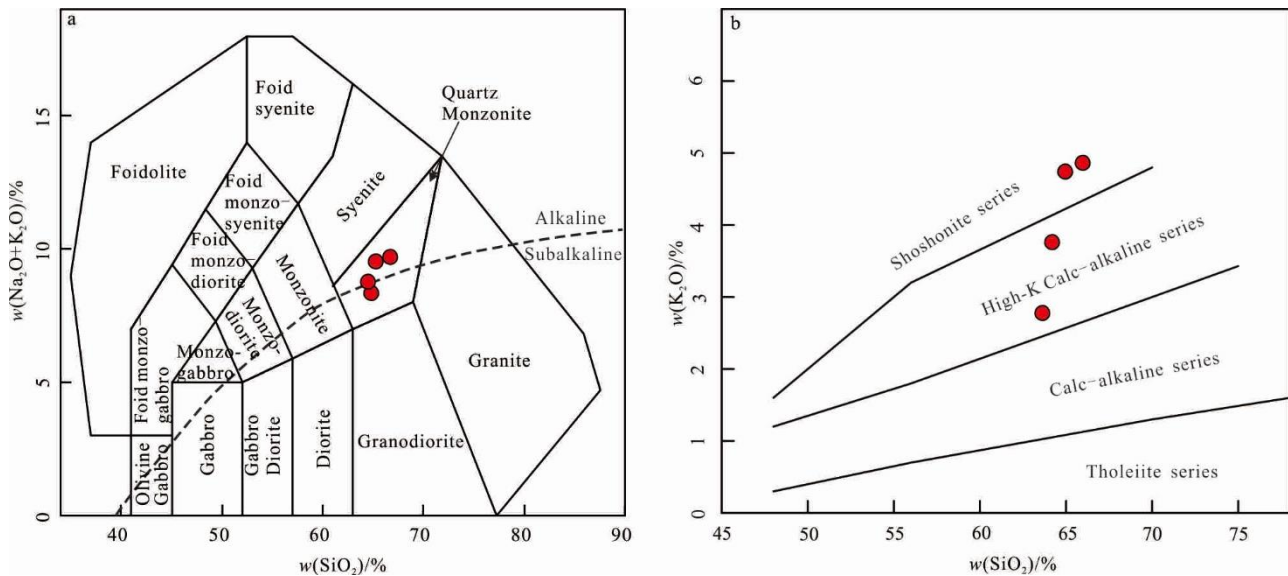


Figure 4. TAS ((a), modified after reference [20]) and $\text{SiO}_2\text{-K}_2\text{O}$ ((b), modified after reference [21]) diagrams of quartz monzonites from the Jinling area, the western Shandong province.

All the samples have no significant Eu anomalies (0.89–1.07) but are enriched in LREEs and depleted in HREEs (Figure 5a). On the primitive-mantle normalized trace element spidergrams (Figure 5b), the samples are enriched in large ion lithophile elements (LILEs, such as Ba, K, and Sr) and are depleted in high-field strength elements (HFSEs, such as Nb, Ta, Ti, and P). The contents of Rb, Y, and Th are from 49.4×10^{-6} to 87.9×10^{-6} , from 10.5×10^{-6} to 12×10^{-6} , and from 4.86×10^{-6} to 7.89×10^{-6} , respectively. Additionally, the samples are enriched in high Sr (433×10^{-6} – 625×10^{-6}) and Ba (822×10^{-6} – 1430×10^{-6}) contents.

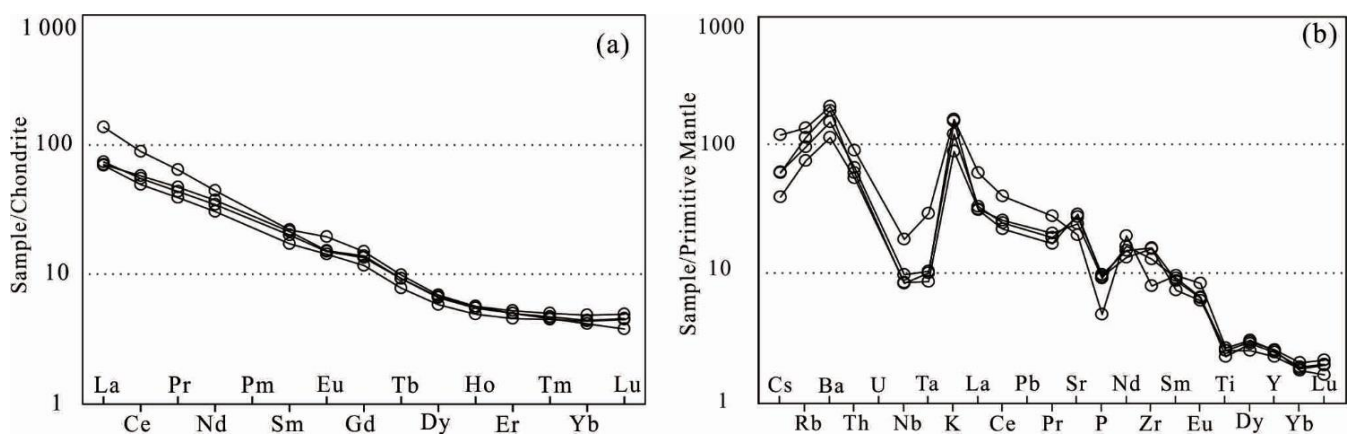


Figure 5. Chondrite normalized rare earth element pattern diagram ((a), after reference [22]) and primitive mantle normalized spider diagram ((b), after reference [23]) of quartz monzonites from the Jinling area, the western Shandong province.

4.4. Sr-Nd-Pb Isotopic Analyses

The whole-rock Sr-Nd-Pb isotopic data are listed in Table 4 and are calculated based on the zircon U-Pb age. The contents of Rb and Sr range from 49.4×10^{-6} to 105×10^{-6} and from 342×10^{-6} to 601×10^{-6} . The values of $^{87}\text{Sr}/^{86}\text{Sr}$ (0.705997–0.706704) are higher than those of the mantle (0.704) [24] and the values of modern values of the primitive mantle (0.7045) [25], while these values are significantly lower than the average $^{87}\text{Sr}/^{86}\text{Sr}$ values of the continental crust (0.7045) [26,27]. The $^{143}\text{Nd}/^{144}\text{Nd}$ ratios are from 0.512068 to 0.512255, lower than the modern values of the primitive mantle (0.512638) [28]. For the samples where $I_{\text{Sr}} = +10.6$ to $+22.0$ and $\epsilon_{\text{Nd}(t)} = -5.93$ to -9.67 , the initial Sr values are from 0.7021 to 0.7059 and lower than the value of 0.706 of basaltic magma formed by mantle [25,29], with a value of 0.718 of granites formed by the partial melting of the crust [26,27]. However, the values of the initial $^{87}\text{Sr}/^{86}\text{Sr}$ and $\epsilon_{\text{Nd}(t)}$ values of quartz monzonites in this study are similar to the initial $^{87}\text{Sr}/^{86}\text{Sr}$ values (0.704726 to 0.704875) and $\epsilon_{\text{Nd}(t)}$ values (-9.5 to -8.6) of quartz monzonites samples in the Jinling area, but the initial $^{87}\text{Sr}/^{86}\text{Sr}$ values are higher than the ones (0.704726 to 0.704875) of gabbro diorites, and the $\epsilon_{\text{Nd}(t)}$ values are lower than the values (-6.4 to -5.4) of gabbro diorites.

Table 4. Sr-Nd-Pb isotopic compositions of the quartz monzonites in the Jinling area, western Shandong province.

Sample	Rb	Sr	$^{87}\text{Rb}/^{86}\text{Sr}$	$^{87}\text{Sr}/^{86}\text{Sr}$	2σ	$(^{87}\text{Sr}/^{86}\text{Sr})_i$	Sm	Nd	$^{147}\text{Sm}/^{144}\text{Nd}$	
HZ7	49.4	529	0.270158	0.706390	0.000009	0.705906	4.23	22.8	0.112147	
HS4	105	342	0.888224	0.706704	0.000007	0.705050	0.75	4.48	0.101740	
HTS3	63.1	601	0.303727	0.705997	0.000008	0.705453	4.02	21.1	0.115168	
Sample	$^{143}\text{Nd}/^{144}\text{Nd}$		$\pm 2\sigma$	$\epsilon_{\text{Nd}}(0)$	$\mathcal{F}(\text{Sm}/\text{Nd})$	$T_{\text{DM}}(\text{Ga})$	$T_{\text{CHUR}}(\text{Ga})$	$^{206}\text{Pb}/^{204}\text{Pb}$	$\pm 2\sigma$	
HZ7	0.512068		0.000009	-9.76	-0.43	1.623	1.027	17.9798	0.0005	
HS4	0.512255		0.000007	-5.89	-0.48	1.220	0.615	17.4543	0.0006	
HTS3	0.512157		0.000007	-8.08	-0.41	1.537	0.900	17.5919	0.0006	
Sample	$^{207}\text{Pb}/^{204}\text{Pb}$		$\pm 2\sigma$	$^{208}\text{Pb}/^{204}\text{Pb}$	$\pm 2\sigma$	$(^{206}\text{Pb}/^{204}\text{Pb})_t$	$(^{207}\text{Pb}/^{204}\text{Pb})_t$	$(^{208}\text{Pb}/^{204}\text{Pb})_t$	$\Delta 7/4$	$\Delta 8/4$
HZ7	15.4332		0.0006	38.1509	0.0018	17.979	15.433	38.150	-0.67	78.70
HS4	15.3898		0.0006	37.6695	0.0017	17.454	15.390	37.669	0.67	94.03
HTS3	15.4074		0.0007	37.5887	0.0022	17.592	15.407	37.588	0.95	69.34

The ratios of initial $^{208}\text{Pb}/^{204}\text{Pb}$, initial $^{207}\text{Pb}/^{204}\text{Pb}$, and initial $^{206}\text{Pb}/^{204}\text{Pb}$ are from 37.75 to 38.15, from 15.41 to 15.43, and from 17.59 to 17.98, respectively. These ratios are similar to the ones of quartz monzonite and higher than the ones of gabbro diorites [10]. With the method of the H–H single-stage Pb evolution model, the Pb isotopic parameters and time of Pb single-stage evolution could be obtained [29]. All the analyzed results are listed in Table 4. Furthermore, the H–H model age is from 275 Ma to 530 Ma, the μ value is 9.18, while the ω and Th/U ratios are from 35.72 to 36.15 and from 3.77 to 3.82, respectively.

5. Discussion

Rock alteration affects the whole-rock geochemistry and isotopic features, leading to the fact that the whole-rock geochemistry and isotopic data could not efficiently reflect the source nature and material source. Therefore, when it comes to the discussion of the nature of magma, it is important to confirm the degree of the sample alteration. In this condition, loss of ignition can signify the degree of the alteration. The loss of ignition of samples in this study is from 0.6% to 1.14%, indicating that Jinling quartz monzonites were slightly affected by the alteration [30]. Meanwhile, the low content of Rb and ratios of Rb/Sr furtherly manifested that the contents of Rb and Sr are limitedly affected by the alteration, while the Sm and Nd isotopes and Hf isotopes in zircons are difficult to be affected by the lateral geological events [31]. In summary, the geochemistry and isotopic data in this paper were limitedly affected by the alteration and could be used to discuss the nature of the magma.

5.1. Petrogenesis and Nature of the Magma Source

The weighted mean age of quartz monzonites (127 ± 1 Ma and 126 ± 1 Ma) is close to the emplacing age of monzonites and biotite diorites (126–128 Ma [9]) and slightly younger than the emplacing age of gabbro diorites (130 Ma~132 Ma, [10]) and quartz monzonites.

Judged by the rock-forming age, all of them are the key parts of Early Cretaceous magmatism outcropped in North China Craton. Based on the geological data and zircon U-Pb dating data, the different lithology of Early Cretaceous magmatism in the Jinling area have a spatiotemporal distributed relationship. In addition, the content of SiO_2 has an obvious linear relationship with the content of MgO , Fe_2O_3^T , P_2O_5 , Al_2O_3 , K_2O , and $\text{Na}_2\text{O} + \text{K}_2\text{O}$ in the Harker diagram (Figure 6). Therefore, the Early Cretaceous quartz monzonites and monzonites in the Jinling area should have the same magma source.

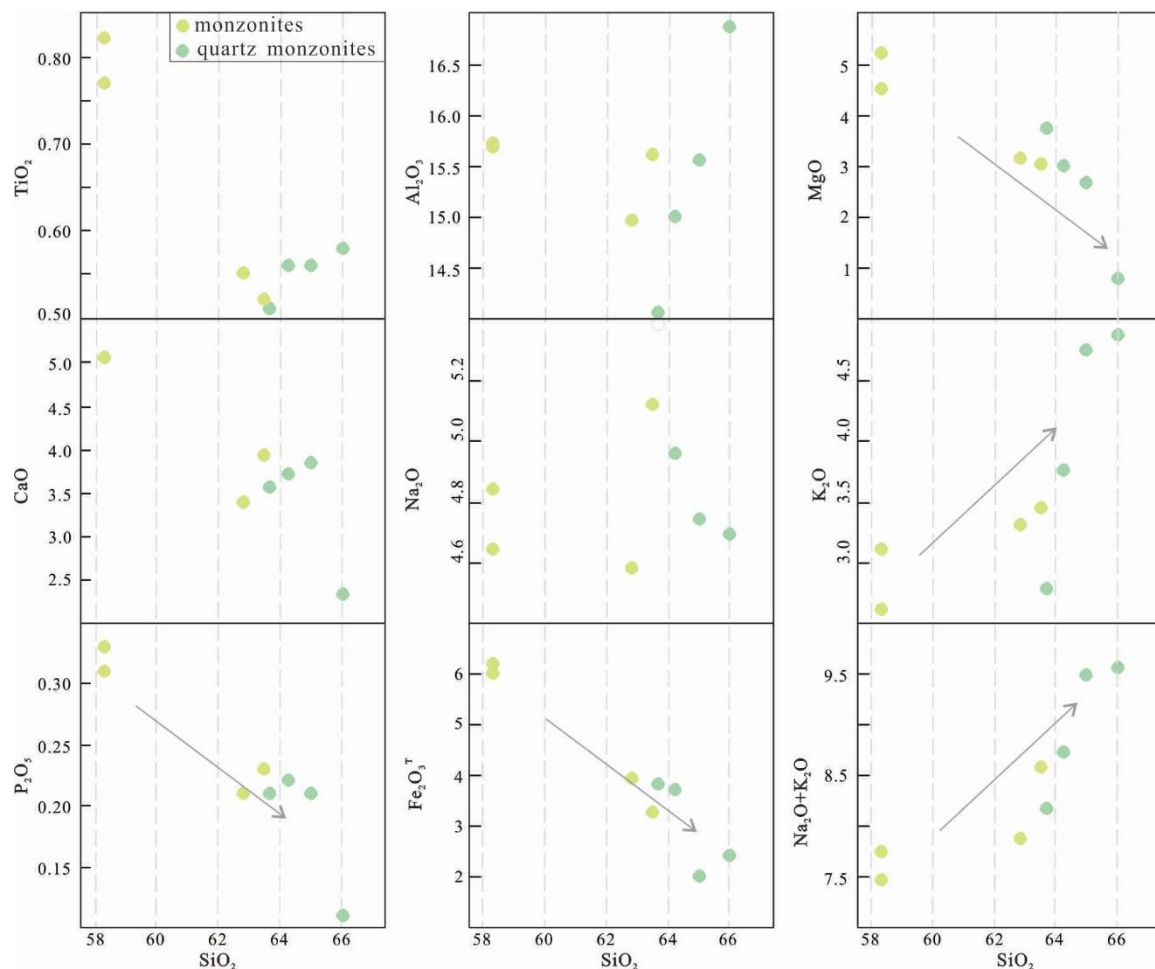


Figure 6. Harker diagram of quartz monzonites and monzonites; the data of monzonites are from reference [11].

The quartz monzonites have SiO_2 content ranging from 63.72% to 66.06% and Al_2O_3 content from 14.04% to 16.86%. The samples with $\text{Mg}^\#$ values from 36 to 70 are featured by high Ni, Cr, and V contents, suggesting the magma source was from the mantle [32]. Combined with the values of μ and w from Pb isotopes, the change of Sr and Nd isotopes could provide important information related to the geological process and could be an efficient way to trace the source characteristics of magmatic rocks [33]. In general, the magmatic rocks with an $^{87}\text{Sr}/^{86}\text{Sr}$ value of >0.710 could be considered as magmatic rocks derived from the crust, while the magmatic rocks with an $^{87}\text{Sr}/^{86}\text{Sr}$ value of <0.705 could be considered as magmatic rocks from the mantle. However, the values of $^{87}\text{Sr}/^{86}\text{Sr}$ in this study are between 0.705 and 0.710, similar to the $^{87}\text{Sr}/^{86}\text{Sr}$ values of intermediate

to basic rocks modified by crust in western Shandong Province. In the Nd-*I*sr diagram (Figure 7a), all the samples are plotted near the field of mantle evolution, displaying the features of mantle magma or juvenile lower crust. The μ value is higher than the one (8.92) of the primitive mantle and lower than the one (9.58) of the upper crust. However, the μ value is similar to the ones of the lower crust or mantle [34–37]. Furthermore, the value of w is lower than the average of the crust, while the Th/U ratio (36.84) is higher than the Th/U ratio (3.45) of the mantle [34]. In the $\Delta\beta$ - $\Delta\gamma$ diagram (Figure 7b), the samples of quartz monzonites are plotted in the field of mantle-derived and orogenic lead, indicating the quartz monzonites have the mantle magmatic properties. Moreover, the samples are plotted near the mantle evolution line, similar to the features of mantle lead. However, the enrichment in LREEs and LILEs is typically different from the features of LREEs and LILEs from the asthenosphere mantle, while the higher initial $^{87}\text{Sr}/^{86}\text{Sr}$ value and lower ϵ_{Nd} value also have typical differences from the ones of the asthenosphere mantle. In summary, the Sr-Nd-Pb isotopic data are similar to the Sr-Nd-Pb features of mantle-derived magma during the same period and are obviously different from the Sr-Nd-Pb features of the North China Craton crust [10]. Combined with the geochemical and isotopic features of kimberlites and peridotites, the quartz monzonites in this study could be the subcontinental lithospheric mantle, which is metasomatized and hydrated [10].

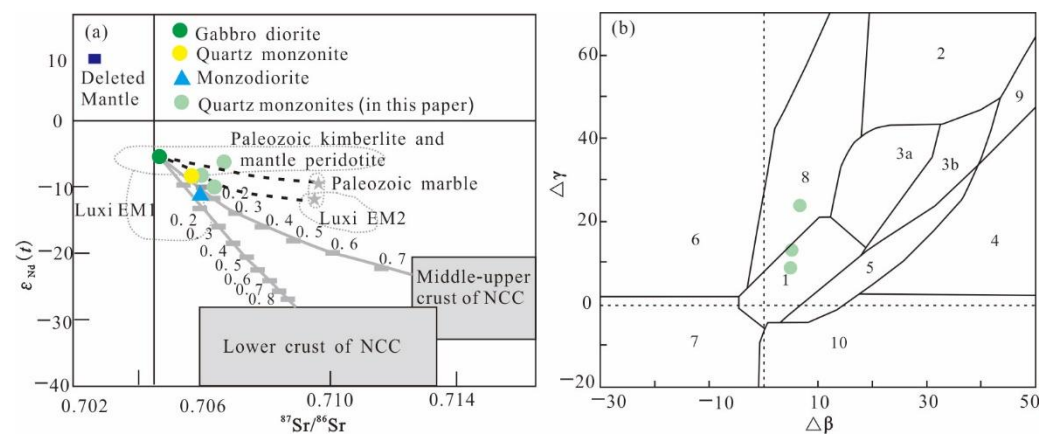


Figure 7. $(^{87}\text{Sr}/^{86}\text{Sr})_i$ vs. $\epsilon_{\text{Nd}(t)}$ diagram (a) and $\Delta\beta$ - $\Delta\gamma$ diagram (b) of quartz monzonites from Jinling area, the western Shandong province. 1—Mantle lead; 2—supracrustal lead; 3—subducted lead from the supracrustal-mantle mixed substances (3a—magmatism; 3b—sedimentation); 4—Chemical deposit lead; 5—submarine hydrothermal lead; 6—medium to deep metamorphic lead; 7—deep metamorphic supracrustal lead; 8—orogenic belt lead; 9—ancient shale subcrustal lead; 10—retrograde metamorphic lead.

Considering the existence of ~ 2.5 Ga zircon in the sample, the magma of the quartz monzonites was influenced by the ancient crust material. The negative $\epsilon_{\text{Hf}(t)}$ value further implies that the magma of the quartz monzonites was influenced by the ancient crust material, while the samples are plotted in the range of chondrite and lower crust evolution line in Figure 8. Previous studies have suggested that the Early Cretaceous lithosphere mantle has been strongly modified by the continental low crust, but the source of crust material is still under debate: (1) the crustal materials of North China [8,38], (2) the crustal materials of South China [37], and (3) the oceanic crustal of Pacific [39,40]. However, the existence of 2.5 Ga zircons indicates the crustal material in the magma should not be the oceanic crustal of the Pacific. The compositions of Pb isotopes could be an efficient indicator to distinguish different tectonic domains. Based on the previous studies, the North China Craton is featured by the low initial isotopic Pb data, while the South China Craton (Yangtze Craton) is characterized by the high initial isotopic Pb data. Furthermore, the values of $^{206}\text{Pb}/^{204}\text{Pb} = 17.8$, $^{207}\text{Pb}/^{204}\text{Pb} = 15.5$, and $^{208}\text{Pb}/^{204}\text{Pb} = 38$ are used as the important signatures to distinguish the basements of North China Craton and South China Craton.

The samples in this study are mainly plotted in the range of compositions of Pb from the lower crustal material of granulite facies in North China (Figure 9), while one sample is plotted in the range of Mesozoic mafic rocks of the Yangtze craton.

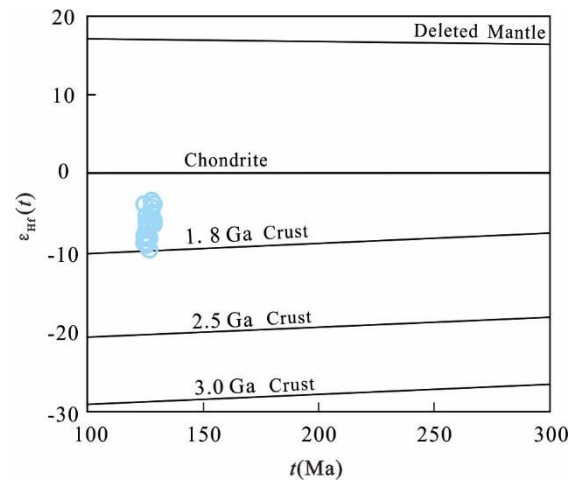


Figure 8. The diagrams of t - $\epsilon_{\text{Hf}}(t)$ of the Jinling complex pluton.

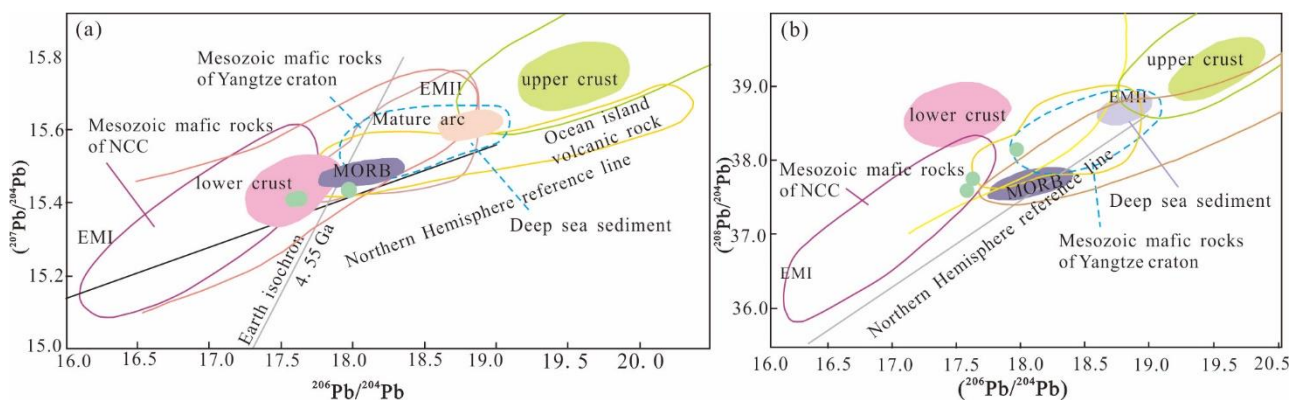


Figure 9. Pb isotopic compositions of the quartz monzonites from the Jinling area, western Shandong province. (a): The diagram of $^{206}\text{Pb}/^{204}\text{Pb}$ vs. $^{207}\text{Pb}/^{204}\text{Pb}$ (b): The diagram of $^{206}\text{Pb}/^{204}\text{Pb}$ vs. $^{208}\text{Pb}/^{204}\text{Pb}$.

Considering the Pb isotopic features and captured zircons, the ancient crust in the magma source in the Jinling area should be mainly from the crustal materials of the North China Craton and was partially influenced by the Yangtze Craton [41]. Although the major elements have a line relationship with the SiO_2 contents, indicating the magma experienced the assimilation and fractional crystallization, the values of $(^{87}\text{Sr}/^{86}\text{Sr})_i$ and ϵ_{Nd} do not show the obviously linear relationship with the SiO_2 contents [10]. However, the lower crust of the North Craton with low Sr and Nd isotopes could not be the ancient crust materials in the parent magma of quartz monzonites (Figure 7a). However, the mixture of primitive magma and 15% to 20% upper crust could be the source magma of quartz monzonites. In summary, the magma of quartz monzonites could originate from the lithospheric mantle and was mixed with the upper crust of the North China Craton.

5.2. Geological Significance

Early Cretaceous magmatic activities are widely distributed in the eastern part of NCC, including Early Cretaceous intrusive rocks (140–110 Ma) and volcanic rocks (135–122 Ma) in the Yanshan–Liaoxi area, Early Cretaceous igneous rocks (130–110 Ma) in the Jiaong area, intermediate-felsic rocks in Jinan–Zibo (~130 Ma) and Fangcheng–Feixian (123–119 Ma)

of western Shandong province, A-type granites in the Liaodong Peninsula and bimodal volcanic rocks in Liaonan–Ji’nan area. Meanwhile, the contemporaneous ductile shear zone and metamorphic core complex are also distributed in Taili, Yiwulvshan, Yunmengshan–Chengde, and Queshan in the eastern part of North China Craton. Thus, the eastern part of North China Craton was likely to be under an extensional geological setting during the Early Cretaceous [42,43]. Furthermore, Cui et al. (2020) [5] have summed up the granitic geochemistry from 160 Ma to 120 Ma and has concluded that the transition time of the tectonic regime from subduction to extension was limited during 139–130 Ma; after 130 Ma, the eastern part of North China Craton was under an extensional geological setting which was characterized by A-type granites, bimodal volcanic rocks, and metamorphic core complex, etc. The samples in this study have been plotted in the active continental margin (Figure 10a,b), while the samples have been plotted in the POG (Figure 10c) and Late-orogenic to post collision uplift (Figure 10d). Considering the regional tectonic setting, the monzonites in the Jinling area were likely formed in an extensional geological setting.

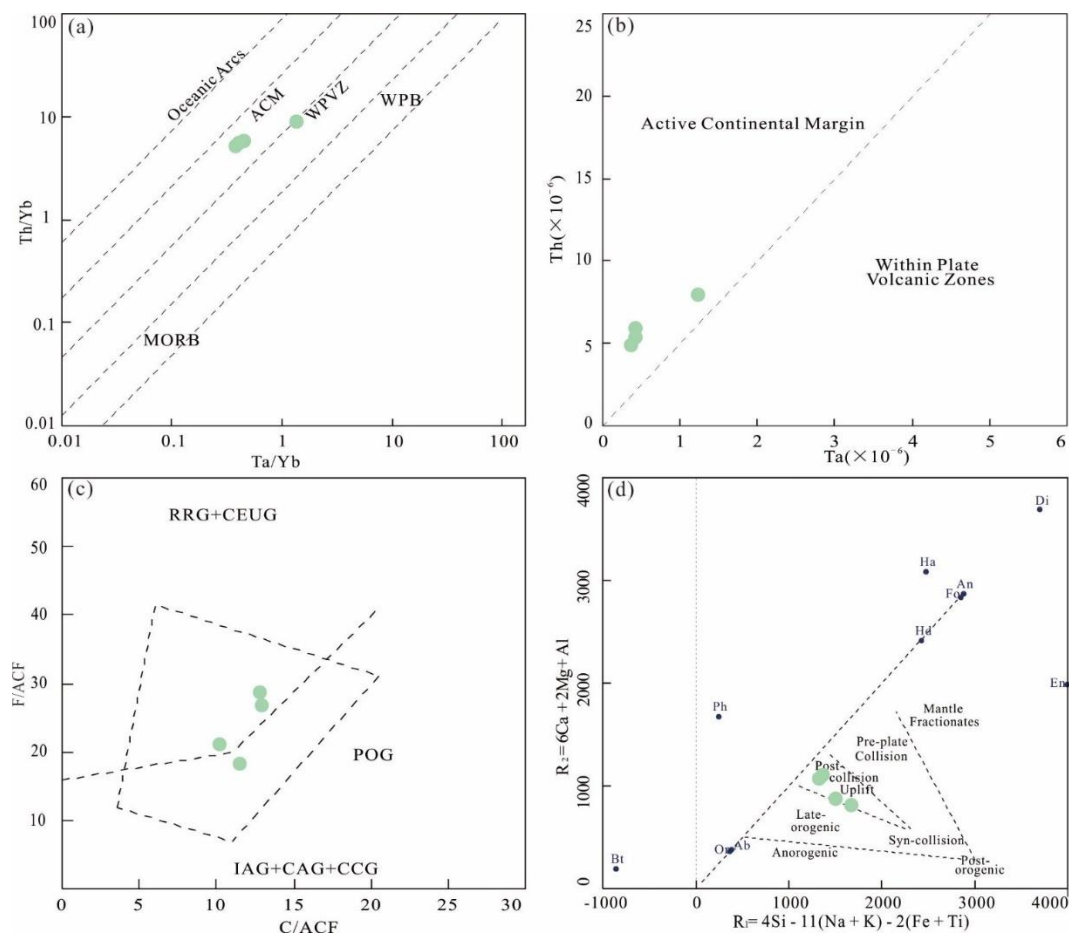


Figure 10. The tectonic setting of the quartz monzonites in the Jiling area, western Shandong province, (a)—the diagrams of Ta/Yb–Th/Yb, (b)—the diagrams of Ta–Th, (c)—the diagrams of C/ACF–F/ACF, (d)—the diagrams of R_1 – R_2 .

Detailed research on the Mesozoic magmatic rocks has revealed that the emplaced age of magmatic rocks in eastern China became younger from the inland to the coasts [5]. These temporal and spatial characteristics of magmatic rocks in eastern China indicate that the extensional setting was likely to be related to the rollback of the Paleo-Pacific. Geological, geophysical, and geochemical features have shown that the destruction and modification occurred widely in the eastern part of North China Craton at ~127 Ma. Considering the emplacement age (~127 Ma) and the geochemistry of the monzonites in the study area, the

monzonites in the Jinling area were formed in an extensional setting, which was linked with the rollback of the Paleo-Pacific (Figure 11).

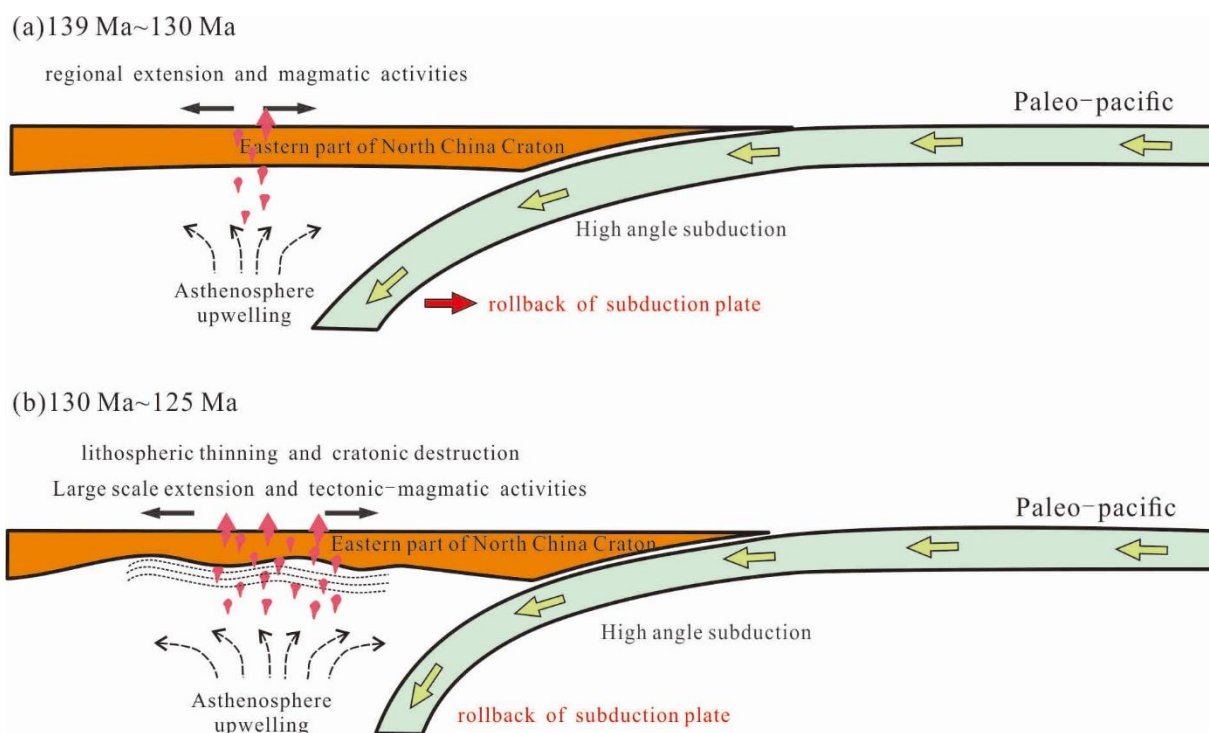


Figure 11. The tectonic setting of the eastern part of the North China Craton from 139 Ma to 125 Ma (modified after reference [5]). (a): The tectonic model for eastern part of North China Craton during 139–130 Ma (b): The tectonic model for eastern part of North China Craton during 130–125 Ma.

6. Conclusions

LA-ICP-MS zircon U-Pb dating indicates that quartz monzonites in the Jinling area formed in the Early Cretaceous (~126 Ma) and was the key part of early Cretaceous magmatic rocks in western Shandong province. These rocks were formed under the back-arc-style extensional setting due to the subduction of the Pacific plate.

The quartz monzonites, with high $Mg^{\#}$ values, Ni contents, Cr contents, and V contents, have an affinity to mantle-sourced rocks. The Sr-Nd isotopic data and zircon Hf isotopic data show that the primary magma of quartz monzonites could be derived from partial melting of lithospheric mantle source and mixed by the upper crustal materials (~15–20%) of North China Craton.

Author Contributions: Conceptualization, Z.-L.Z., C.Z. and J.-L.G.; Data curation, Z.-L.Z. and Y.L.; Formal analysis, M.M.; Funding acquisition, Y.-D.L.; Methodology, Z.-L.Z., C.Z., Y.L. and J.-L.G.; Project administration, Z.-L.Z. and C.Z.; Software, Z.-L.Z., Y.L. and L.-Y.W.; Validation, Y.L., L.-Y.W. and J.-L.G.; Writing—original draft, Z.-L.Z. and C.Z.; Writing—review and editing, Z.-L.Z., C.Z. and J.-L.G. All authors have read and agreed to the published version of the manuscript.

Funding: This research was funded by the National Science Foundation of Shandong Province (ZR2021MD104, ZR2019PD010), the National College Students' Innovation and Entrepreneurship Training Program (202110433021), and Science and technology research project of Shandong Bureau of Geology and Mineral Resources (KY202201, KC201901).

Acknowledgments: We acknowledge the detailed comments of anonymous journal reviewers and the help of the Guizhou Tongwei Analytical Technology Corporation.

Conflicts of Interest: The authors declare no conflict of interest.

References

1. Yang, J.H.; Wu, F.Y.; Chung, S.L.; Wilde, S.A.; Chu, M.F.; Lo, C.H.; Song, B. Petrogenesis of Early Cretaceous intrusions in the Sulu ultrahigh-pressure orogenic belt, east China and their relationship to lithospheric thinning. *Chem. Geol.* **2005**, *222*, 200–231. [[CrossRef](#)]
2. Zheng, Y.F.; Xu, Z.; Zhao, Z.F.; Dai, L.Q. Mesozoic mafic magmatism in North China: Implications for thinning and destruction of cratonic lithosphere. *Sci. China Earth Sci.* **2018**, *48*, 379–414. (In Chinese) [[CrossRef](#)]
3. Zhu, R.X.; Chen, L.; Wu, F.Y.; Liu, J.L. Timing, scale and mechanism of the destruction of the North China Craton. *Sci. China Earth Sci.* **2011**, *41*, 583–592. (In Chinese) [[CrossRef](#)]
4. Zhu, R.R.; Xu, Y.G. The subduction of the west Pacific plate and the destruction of the North China Craton. *Sci. China Earth Sci.* **2019**, *49*, 1346–1356. (In Chinese) [[CrossRef](#)]
5. Cui, F.H.; Xu, X.C.; Zheng, C.Q.; Yao, W.G.; Shi, L. The paleo-Pacific plate subduction and slab roll-back beneath eastern North China Craton: Insights from the Late Mesozoic granitoids in Xingcheng area, western Liaoning Province. *Acta Petrol. Sin.* **2020**, *36*, 2463–2492. (In Chinese)
6. Zhang, C.; Cui, F.H.; Geng, R.; Zhang, Z.L.; Gao, M.B.; Gao, L.L. The Petrogenesis of Early Cretaceous Quartz Diorite in Skarn Iron Deposits, Jinling Area, Luxi: Evidence of Geochronology and Geochemistry. *Mineral. Petrol.* **2021**, *41*, 80–92. (In Chinese)
7. Yang, C.H.; Xu, W.L.; Yang, D.B.; Liu, C.C.; Liu, X.M.; Hu, Z.C. Petrogenesis of the mesozoic High-Mg diorites in West Shandong: Evidence from chronology and petro-geochemistry. *Earth Sci. J. China Univ. Geosci.* **2006**, *31*, 81–92. (In Chinese)
8. Zhong, J.W.; Huang, X.L. Spatial variation of zircon Hf isotopes for the Early Cretaceous mafic intrusions in western Shandong and its genesis. *Geotecton. Metallog.* **2012**, *36*, 572–580. (In Chinese)
9. Jin, Z.L.; Zhang, Z.C.; Hou, T.; Santos, M.; Liu, H. Genetic relationship of high-Mg dioritic pluton to iron mineralization: A case study from the Jinling skarn-type iron deposit in the North China Craton. *J. Asian Earth Sci.* **2015**, *113*, 957–979. [[CrossRef](#)]
10. Lan, T.G.; Hu, R.Z.; Chen, Y.H.; Tang, Y.W.; Liu, L. Generation of high-Mg diorites and associated iron mineralization within an intracontinental setting: Insights from ore-barren and ore-bearing intrusions in the eastern North China Craton. *Gondwana Res.* **2019**, *72*, 97–119. [[CrossRef](#)]
11. Zhang, C.; Cui, F.H.; Zhang, Z.L.; Geng, R.; Song, M.C. Petrogenesis of Ore-Bearing Dioritic Pluton in Jinling Area in Western Shandong: Evidence from Zircon U-Pb Chronology and Petro-Geochemistry. *J. Jilin Univ.* **2017**, *47*, 1732–1745. (In Chinese)
12. Wiedenbeck, M.; Allé, P.; Corfu, F.; Griffin, W.L.; Meier, M.; Oberli, L.; Roddick, J.C.; Spiegel, W. Three natural zircon standards for U–Th–Pb, Lu–Hf, trace element and REE analyses. *Geostand. Newsl.* **1995**, *19*, 1–23. [[CrossRef](#)]
13. Slama, J.; Kosler, C.; Crowley, D.J.; Gerdes, J.L.A.; Hanchar, J.M.; Horstwood, M.S.; Morris, G.A.; Nasdala, L.; Norberg, N. Plešovice zircon—a new natural reference material for U–Pb and Hf isotopic microanalysis. *Chem. Geol.* **2008**, *249*, 1–35. [[CrossRef](#)]
14. Vermeesch, P. IsoplotR: A Free and Open Toolbox for Geochronology. *Geosci. Front.* **2018**, *9*, 224–238. [[CrossRef](#)]
15. Wu, F.Y.; Yang, Y.H.; Xie, L.W.; Yang, J.H.; Xu, P. Hf isotopic compositions of the standard zircons and baddeleyites used in U–Pb geochronology. *Chem. Geol.* **2006**, *234*, 105–126. [[CrossRef](#)]
16. Wu, F.Y.; Li, X.H.; Zheng, Y.F.; Gao, S. Lu–Hf isotopic systematics and their Applications in Petrology. *Acta Petrol. Sin.* **2007**, *23*, 185–220. (In Chinese)
17. Jitka, M.; Petra, D. Modified chromatographic separation scheme for Sr and Nd isotope analysis in geological silicate samples. *J. Geosci.* **2007**, *52*, 221–226.
18. Collerson, K.D.; Balz, S.K.; Ronny, S. Applications of accurate, high-precision Pb isotope ratio measurement by multi-collector ICP-MS. *Chem. Geol.* **2002**, *188*, 65–83. [[CrossRef](#)]
19. Collerson, K.D.; Marshall, I.W. Stone adze compositions and the extent of ancient Polynesian voyaging and trade. *Science* **2007**, *317*, 1907–1911. [[CrossRef](#)]
20. Irvine, T.H.; Baragar, W.R.A. A guide to the chemical classification of the common volcanic rocks. *Can. J. Earth Sci.* **1971**, *8*, 523–548. [[CrossRef](#)]
21. Peccerillo, A.; Taylor, A.R. Geochemistry of Eocene calc-alkaline volcanic rocks from the Kastamonu area, Northern Turkey. *Contrib. Miner. Petrol.* **1976**, *58*, 63–81. [[CrossRef](#)]
22. Boynton, W.V. Geochemistry of the rare earth elements: Meteorite studies. In *Rare Earth Element Geochemistry*; Henderson, P., Ed.; Elsevier: Amsterdam, The Netherlands, 1984; pp. 63–114.
23. Sun, S.S.; McDonough, W.F. Chemical and isotopic systematics of oceanic basalts: Implications for mantle composition and processes. *Geol. Soc.* **1989**, *42*, 313–345. [[CrossRef](#)]
24. Faure, G. *Principles of Isotope Geology*; John Wiley & Sons: New York, NY, USA, 1986; Volume 2, pp. 141–247.
25. Depaolo, D.J.; Wasserburg, G.J. Inferences about magma sources and mantle structure from variations of $^{143}\text{Nd}/^{144}\text{Nd}$. *Geophys. Res. Lett.* **1976**, *3*, 743–746. [[CrossRef](#)]
26. Sun, S.L. The Study on Metallogenic series of Hydrocarbon Alkali-Fluids. In *Devonian in Xicheng Concentrated Mineralization Area, West Qinling, Gansu Province*; Chengdu University of Technology: Chengdu, China, 2001; pp. 43–44. (In Chinese)
27. Xiao, Q.H.; Deng, J.F.; Ma, D.Q. *Research Ideas and Methods of Granite*; Geological Publishing House: Beijing, China, 2002; pp. 71–120. (In Chinese)
28. Jacobsen, S.B.; Wasserburg, G.J. Sm–Nd isotopic evolution of chondrites and achondrites. *J. Petrol.* **1984**, *67*, 137–150. [[CrossRef](#)]
29. Faure, G.; Mensing, T.M. *Isotopes: Principles and Applications*; John Wiley & Sons: New York, NY, USA, 2005; Volume 3, pp. 256–283.

30. Ding, L.X.; Huang, G.C.; Xia, J.L. Age and Petrogenesis of the Echeng Intrusion in Southeastern Hubei Province: Implications for Iron Mineralization. *Earth Sci.* **2018**, *43*, 2350–2369. (In Chinese)
31. Griffin, W.L.; Wang, X.; Jackson, S.E.; Pearson, N.J.; Suzanne, Y.O.; Reilly, A.; Xu, X.S.; Zhou, X.M. Zircon chemistry and magma mixing, SE China: In-situ analysis of Hf isotopes, Tonglu and Pingtan igneous complexes. *Lithos* **2002**, *61*, 237–269. [[CrossRef](#)]
32. Rapp, R.P.; Watson, E.B. Dehydration Melting of Metabasalt at 8–32 kbar: Implications for Continental Growth and Crust-Mantle Recycling. *J. Petrol.* **1995**, *36*, 891–931. [[CrossRef](#)]
33. Lv, P.R.; Li, D.R.; Peng, Y.W.; Zhang, M.Y. S-Pb characteristics of ore sulfides and U-Pb dating of zircon from the Sankuanggou Skarn-type Cu-Fe-Mo deposit in Heilongjiang Province. *Geol. China* **2012**, *39*, 717–728. (In Chinese)
34. Lv, P.R.; Yao, W.G.; Zhang, H.D.; Yu, X.L.; Yang, B.; Meng, G.; Tian, H. Pb,Sr,Nd Isotopic Compositions of the Diorites from Typical Deposits in Reko Dig Porphyry Cu-Au-Ore-Concentrated Area, Pakistan and Their Tracer Significances. *Acta Geol. Sin.* **2016**, *90*, 2803–2817. (In Chinese)
35. Stacey, J.S.; Kramers, J.D. Approximation of terrestrial lead isotope evolution by a two-stage model. *Earth Planet. Sci. Lett.* **1975**, *26*, 207–221. [[CrossRef](#)]
36. Kamona, F.A.; Lévêque, J.; Friedrich, G.H.; Haack, U. Lead isotopes of the carbonate-hosted Kabwe, Tsumeb, and Kipushi Pb-Zn-Cu sulphide deposits in relation to Pan African orogenesis in the Damaran-Lufilian Fold Belt of Central Africa. *Miner. Depos.* **1999**, *34*, 273–283. [[CrossRef](#)]
37. Yang, Q.L.; Zhao, Z.F.; Zheng, Y.F. Slab-mantle interaction in continental subduction channel: Geochemical evidence from Mesozoic gabbroic intrusives in southeastern North China. *Lithos* **2012**, *155*, 442–460. [[CrossRef](#)]
38. Wang, Q.; Wyam, D.A.; Xu, J.F.; Zhao, Z.H.; Jian, P.; Zi, F. Partial melting of thickened or delaminated lower crust in the middle of eastern China: Implications for Cu-Au mineralization. *J. Geol.* **2007**, *115*, 149–161. [[CrossRef](#)]
39. Liu, Y.S.; Gao, S.; Hu, Z.C.; Gao, C.G.; Zong, K.Q.; Wang, D.B. Continental and oceanic crust recycling- induced melt-peridotite interactions in the Trans-North China Orogen: U-Pb dating, Hf isotopes and trace elements in zircon from mantle xenoliths. *J. Petrol.* **2010**, *51*, 537–571. [[CrossRef](#)]
40. Chen, L.H.; Zhou, X.H. Subduction-related metasomatism in the Thinning Lithosphere: Evidence from a composite Dunite-orthopyroxenite Xenolith entrained in Mesozoic Laiwu High-Mg diorite, North China Craton. *Geochem. Geophys. Geosyst.* **2005**, *6*, 301–325. [[CrossRef](#)]
41. Yang, C.H.; Xu, W.L.; Yang, D.B.; Wang, W.; Wang, W.D.; Liu, J.M. Genesis of the Shangyu gabbro diorite in western Shandong Province: The evidences from Geochronology and Geochemistry. *Sci. China Earth Sci.* **2008**, *38*, 44–55. (In Chinese)
42. Yang, H.T.; Yang, D.B.; Shi, J.P.; Xu, W.L.; Wang, F.; Chen, Y. Nature of the Early Cretaceous lithospheric mantle in western Shandong: Constraints from geochronology, geochemistry and Sr-Nd-Ph-Hf isotopic data of Dakunlun gabbros and diabases. *Acta Petrol. Sin.* **2018**, *34*, 3327–3340. (In Chinese)
43. Zhang, Z.C.; Hou, T.; Santosh, M.; Li, H.M.; Li, J.W.; Zhang, Z.H.; Song, X.Y.; Wang, M. Spatio-temporal distribution and tectonic settings of the major iron deposits in China: An overview. *Ore Geol. Rev.* **2014**, *57*, 247–263. [[CrossRef](#)]